Electrically Small, Single-Substrate Huygens Dipole Rectenna for Ultra-Compact Wireless Power Transfer Applications

Wei Lin, *Senior Member, IEEE* and Richard W. Ziolkowski, *Life Fellow, IEEE*

***Abstract*—An electrically small, single-substrate Huygens dipole rectenna with exceptional physical and radiation performance characteristics is reported. A highly efficient rectifier circuit is seamlessly integrated with an ultra-thin, electrically small, Huygens dipole antenna (HDA) on a single piece of Rogers™ 5880 substrate. It consists of two metamaterial-inspired near-field resonant parasitic (NFRP) elements, an Egyptian axe dipole (EAD) and a capacitively loaded loop (CLL), that are etched, respectively, on the top and bottom metallization layers of the substrate. A printed receiving dipole is amalgamated tightly with the rectifier on the CLL layer. This ultra-compact rectenna system has a large electromagnetic wave capture capability and achieves nearly complete conversion of the incident energy into DC power. The HDA prototype has a realized gain of 4.6 dBi and a half power beamwidth (HPBW) greater than 130˚. The entire rectenna is electrically small with *ka* = 0.98, is low cost and easy to fabricate, and has a measured 88% AC to DC conversion efficiency. The developed rectenna system is the ideal candidate for ultra-compact far-field wireless power transfer (WPT) applications.**

***Index Terms*—Electrically small antennas, Huygens dipole antennas, Internet-of-Things (IoT), rectennas, sensors, wireless power transfer (WPT).**

I. Introduction

Wireless Internet-of-Things (IoT) systems and their associated applications have undergone rapid development in the past decade [1] – [3]. Along with the anticipated exponential growth in the number of IoT devices in the 5G era, far-field wireless power transfer (WPT) [4], [5] has become a tactical trend to empower IoT devices. The WPT approach has many desirable advantages over the current usage of short-life, bulky, and weighty batteries.

A rectenna is the most critical component of far-field WPT applications. Extensive research has been conducted on the design of linearly polarized (LP) [6] – [16], dual-polarized [17], [18] and circularly polarized (CP) [19] – [22] rectennas. Nonetheless, it is very challenging to achieve simultaneously an electrically small size ($ka < 1$, where k is the wave number and a is the radius of the smallest sphere enclosing the rectenna); large wireless power capture capacity through high antenna realized gain and large half power beamwidths; and high AC to DC conversion efficiencies.

To address these challenges and to achieve all the described features simultaneously, we have successfully developed several electrically small Huygens rectennas [23] – [25]. However, all of these designs require at least three PCB substrates, two metallic vias, and time consuming manual assembly processes. Their mass production is not feasible. For the future ubiquitous IoT era, it is highly desired to achieve ultra-compact, low cost, and easily fabricated rectennas with excellent wireless power capture capability and conversion efficiency.

We report in this communication the first realized single-substrate Huygens dipole rectenna for ultra-compact WPT applications. Significantly, the entire rectenna is realized on a single piece of Rogers™ 5880 substrate with a thickness of only 0.508 mm. It is the seamless integration of a planar electrically small Huygens dipole antenna (HDA) and a compact, highly efficient rectifier circuit. The HDA consists of two metamaterial-inspired near-field resonant parasitic (NFRP) structures: a capacitively loaded loop (CLL) that acts as the magnetic dipole and an Egyptian axe dipole (EAD) that acts as the electric one. The CLL and EAD structures are etched from opposite copper sides of the substrate. A short dipole element is amalgamated tightly with a very compact rectifier. Both lie on the same side of the substrate as the CLL element. The length of the dipole is specially designed to achieve an inductive impedance from the entire HDA that is a direct conjugate match to the capacitive impedance of the rectifier circuit. The system was designed to operate at 915 MHz in the ISM (Industrial, Scientific, and Medical) band. A prototype of the rectenna was fabricated and tested. It is electrically small with ka = 0.98. The measured results confirm their simulated values. The AC to DC conversion efficiency of the rectenna is a high 88%. It has a large wireless power capture capacity, i.e., its antenna has a realized gain of 4.6 dBi and a half power beamwidth (HPBW) greater than 130˚.

This communication is organized as follows. Sec. II discusses the design and performance of the electrically small, single-substrate HDA. Sec. III presents the design, realization and measurement results of the corresponding prototype rectenna system. Finally, Sec. IV draws some conclusions.

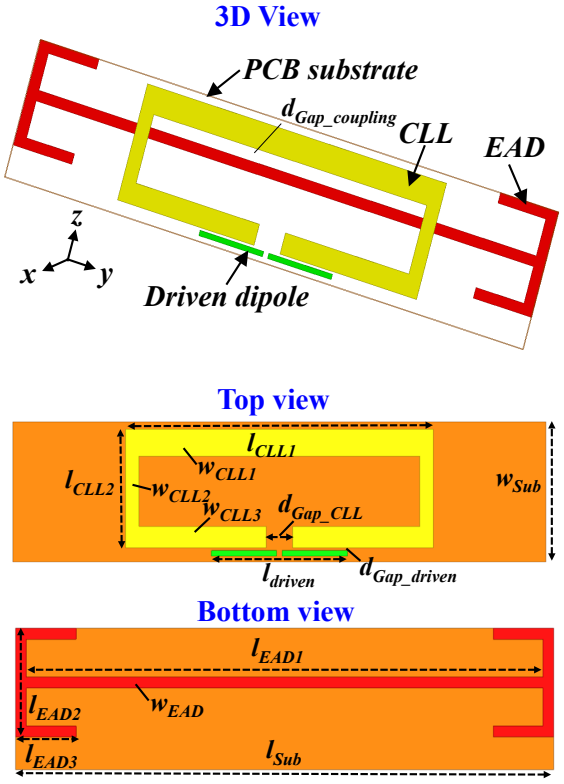

Fig. 1. Configuration of the planar electrically small single-substrate Huygens dipole antenna and its design parameters.

Manuscript received March 11, 2020; This work was supported by the UTS Chancellor's Postdoctoral Fellowship under Grant PRO18-6147.

The authors are with the Global Big Data Technologies Centre, School of Electrical and Data Engineering, University of Technology Sydney, Ultimo, NSW 2007, Australia (email: Wei.Lin@uts.edu.au; Richard.Ziolkowski@uts.edu.au)

II. Single-Substrate Electrically Small HDA Design

A. Antenna configuration and operating mechanisms

The planar electrically small single-substrate HDA configuration is shown in Fig. 1. The noticeable difference of this design from our previously reported electrically small HDAs [26] – [28] is that it is realized on a single piece of thin substrate. The substrate selected is the Rogers™ 5880 copper-cladded laminate whose thickness is 0.508 mm and whose relative permittivity is 2.2 and loss tangent is 0.0009. The metamaterial-inspired CLL and EAD elements are etched on opposite sides of the substrate. A short printed dipole is etched on the same side as the CLL element, close to it, and oriented parallel to its gap. The entire antenna structure is electrically small, e.g., $ka = 0.98 < 1$. It is very easily fabricated with standard PCB manufacturing technologies. The cost is minimal. The detailed dimensions of the optimized design are listed in Table I.

TABLE I:
Planar Electrically Small Huygens Antenna Parameters
(dimensions in millimeters)

Parameter	Description	Value
l_{Sub}	Length of the substrate	99.5
w_{Sub}	Width of the substrate	26.0
l_{CLL1}	Length of the upper CLL	57.4
w_{CLL1}	Width of the upper CLL	5.0
l_{CLL2}	Length of the lateral CLL	22.0
w_{CLL2}	Width of the lateral CLL	2.5
w_{CLL3}	Width of the bottom CLL	4.0
d_{Gap_CLL}	Gap of the CLL	5.0
l_{driven}	Length of the driven dipole	25.4
w_{driven}	Width of the driven dipole	1.0
d_{Gap_driven}	Gap between driven dipole and CLL	0.5
l_{EAD1}	Length of the center EAD	95.5
l_{EAD2}	Length of the lateral EAD	20.0
l_{EAD3}	Length of the bent EAD	11.2
W_{EAD}	Width of the EAD	2
$d_{Gap\_coupling}$	Gap between the EAD and CLL	2.6

The principal operating mechanism of the HDA is the successful excitation of the two NFRP elements, which then produce magnetic and electric dipoles oriented orthogonal to each other. As a transmitting antenna, the short dipole is driven. Its field induces a loop current on the CLL, which acts as the magnetic dipole. The EAD is mainly excited through its coupling to the currents flowing along the upper metallic strip of the CLL; it acts as the electric dipole. By carefully adjusting the couplings between the NFRP and driven elements, the magnetic and electric dipoles amplitudes become balanced. The proper relative phase between the NFRP elements to achieve the broadside cardioid pattern pointed away from the driven dipole is obtained by adjusting the coupling distance parameter $d_{Gap\_coupling}$. Its operation as a receiving antenna follows by reciprocity.

The current distributions on the CLL and EAD for one time period corresponding to its resonance frequency, 915 MHz, are shown in Fig. 2. The induced currents in Figs. 2(a) and 2(c) are strong on both the CLL and EAD elements. The strongest currents on the CLL are found on its upper strip and are oriented opposite to those on the EAD. Consequently, the resulting electric fields reinforce in the desired broadside direction and cancel in the direction towards the driven dipole. These current orientations also yield a nearly uniform loop current distribution because they cancel unwanted non-uniform current components when $d_{Gap\_coupling}$ is optimized. Figs. 3(b) and 3(d) indicate that the EAD currents are still strong, but that the CLL currents are now weak. Hence, they are actually out-of-phase by 90˚. Consequently, the corresponding electric and magnetic dipole current moments are correctly in-phase to obtain the cardioid pattern.

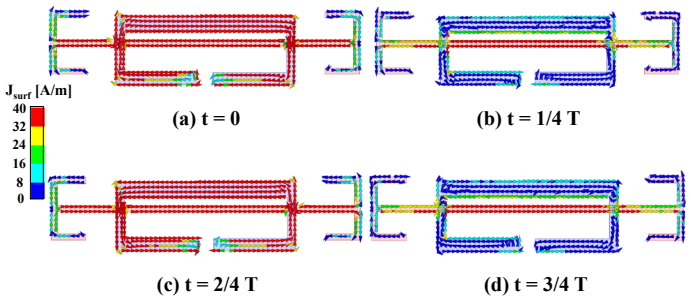

Fig. 2. Current distributions on the CLL and EAD elements in one period, T, corresponding to its resonance frequency, 915 MHz.

The simulated performance characteristics of the HDA are given in Fig. 3. The simulated $|S_{11}|$ and realized gain values as functions of the source frequency in Fig. 3(a) indicate that the antenna is resonating at 915 MHz and that the peak realized gain is 4.6 dBi there. The Huygens cardioid radiation patterns are realized as shown in Fig. 3(b). They are almost identical in the two vertical planes, $\varphi = 0^\circ$ and $\varphi = 90^\circ$. The HPBW = ±67˚, i.e., the 3−dB beam coverage is 134˚.

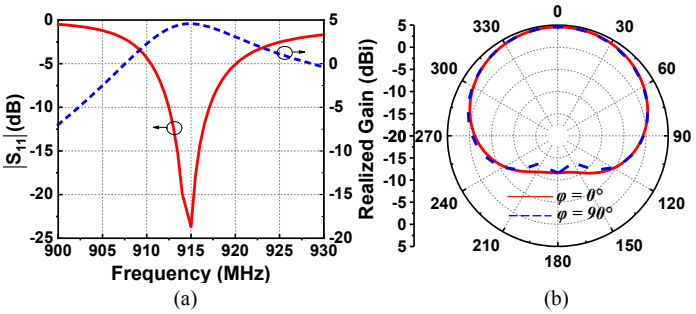

Fig. 3. Simulated results. (a) $|S_{11}|$ and realized gain values as functions of the source frequency. (b) Radiation patterns in the two vertical planes at 915 MHz.

B. Critical design considerations

There are two critical design parameters. One is the gap, $d_{Gap\_coupling}$, between the EAD and the CLL. This gap determines the coupling between these two NFRP radiators and affects both the overall impedance matching and radiation patterns. The associated parameter studies are summarized in Fig. 4. Figs. 4(a) and 4(b) indicate that the resonance frequency shifts from 907 to 922 MHz when the gap changes from 2.4 to 2.8 mm. Figs. 4(c) and 4(d) illustrate that good Huygens patterns that are identical in both vertical planes occur only when the gap is 2.6 mm. Large discrepancies are found when the gap is either 2.4 or 2.8 mm. Thus, the gap value was 2.6 mm for the optimized design.

Another concern is to remove as many circuit components as possible to minimize losses and, hence, the lossy lumped inductor between the HDA and the rectifier in particular. Because the rectifier has a large capacitive reactance, the HDA was redesigned to have a large inductive input impedance that was a direct conjugate match to the rectifier. This efficiency-critical feature was simply achieved by increasing the length of the small dipole. Fig. 5 shows the input impedance for different lengths: 24.2, 25.4, and 26.6 mm, as functions of the source frequency. While the imaginary part changes noticeably near the targeted frequency of 915 MHz, the real part only exhibits a slight variation. The length, l_{driven} = 26.6 mm, in the final design yielded the required input impedance: 55 + j112 Ω.

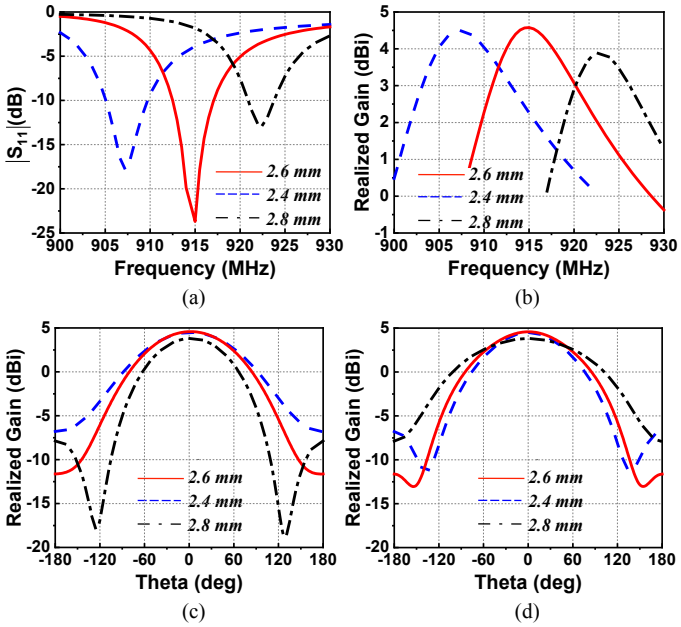

Fig. 4. Parameter studies of the coupling distance $d_{Gap\_coupling}$ between the EAD and the CLL. (a) $|S_{11}|$ and (b) realized gain values as functions of the source frequency; Radiation patterns in (c) $\varphi = 0^{\circ}$ and (d) $\varphi = 90^{\circ}$ planes.

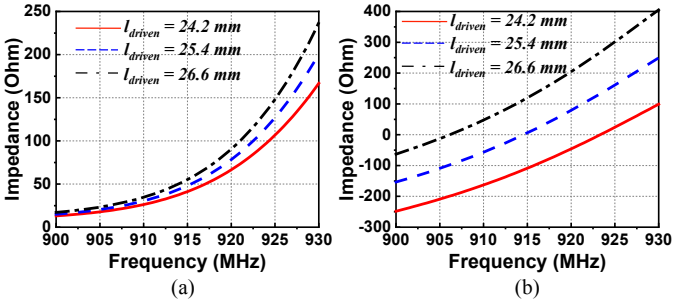

Fig. 5. Parameter studies of the HDA's input impedance for different lengths of its short dipole. (a) Real part. (b) Imaginary part.

C. *Design guidelines*

The developed HDA design is suited for tuning to an arbitrary frequency of operation f_0. The design guidelines are summarized as follows. The first step is to design the CLL and the associated short driven dipole. The total length of the CLL is initially set to be 0.2 λ_0. The initial width of its top and bottom is initially 0.01 λ_0. The short driven dipole must be placed close to the CLL gap and parallel to it. The initial values for the gap and the width of the dipole are, respectively, 1/10 and 1/4 of the width of the bottom strip of the CLL. The length of the dipole is then adjusted to yield a resonance frequency around 8% higher than f_0. The second step is to design the EAD. The initial total length of the EAD ($l_{EAD1} + 0.5l_{EAD2} + l_{EAD3}$) is 0.43 λ_0; its width is half that of the upper CLL strip. The EAD is then placed close to the upper strip of the CLL with $d_{Gap\_coupling} \approx 0.008\ \lambda_0$. The third step is to fine-tune this gap distance along with the length and width of the EAD through simulations until an acceptable Huygens performance is achieved at f_0.

III. Electrically Small Single-Substrate Huygens Rectenna System

A. *System Configuration*

The rectenna shown in Fig. 6 was realized by seamlessly integrating the indicated rectifier with the developed single-substrate HDA. The rectifier itself is compact and implemented on a co-planar microstrip line with lumped components. The latter include two Schottky diodes, three capacitors, two inductors and one resistor. The main components of this full-wave rectifying circuit are the two Schottky diodes, D_1 and D_2, which act as a voltage doubler. They are a package type HSMS286C from Broadcom™. The capacitors C_1 and C_2 acts as a matching network between the voltage doubler and the HDA. The inductive impedance of HDA prevents any harmonics from the diodes being re-radiated. The capacitor C_2 works as an energy storage component during each negative period of the received sinusoidal wave. The capacitor C_3 acts as a low-pass filter that smooths the output DC voltage. The resistor R_L is the load and the two inductors L_{c1} and L_{c2} act as RF chokes. The entire rectifier is very compact having a total length of only 1.0 cm. The actual values of its components are: C_1 = 0.4 pF, $C_2 = C_3$ 100 pF, R_L = 5.1K Ω, $L_{c1} = L_{c2}$ = 560 nH. As noted earlier, the input impedance of the antenna is designed to have the inductive value, 55 + j112 Ω, i.e., to be conjugately matched to the rectifier. This feature eliminates the need to include a very lossy inductor to act as the matching element.

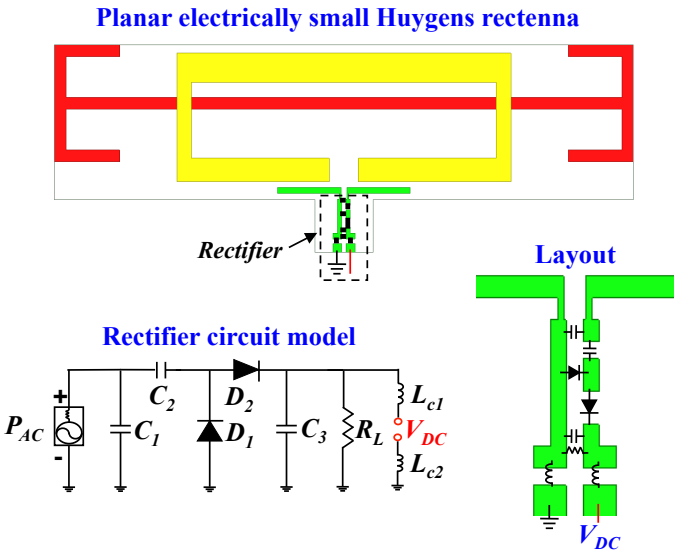

Fig. 6. System configuration of the ultra-compact, single-substrate Huygens dipole rectenna, emphasizing its rectifying circuit model and layout.

B. *Fabricated prototype and measured results*

The optimized rectenna was fabricated as the photos in Fig. 7 show. The entire prototype is ultra-compact, lightweight, low-cost and easy to fabricate. The metallization layers of the rectenna were etched by standard and low cost PCB manufacturing technology. The lumped components of the rectifier were easily soldered manually in the prototype. Mass production is very feasible with industrial soldering processes.

The rectenna prototype was tested in an anechoic chamber with the customized far-field measurement setup shown in Fig. 8. The wireless power was generated by a signal generator from Keysight Technologies™. This signal was magnified via a power amplifier, type ZHL-20W-13SW+ from Mini-Circuits™, and then delivered to a broadband (800 MHz to 18 GHz) double-ridge horn antenna. Two coaxial cables interconnected these three devices and a DC supply source was used to power the amplifier. The horn antenna emitted the electromagnetic waves that were incident on the rectenna. A multimeter was adopted to measure the output DC voltage V_o of the rectenna. From the Friis transmission equation [29]:

$$\frac{P_r}{P_{in}} = G_t \times G_r \times \left(\frac{\lambda_0}{4\pi R}\right)^2 \quad (1)$$

the received power P_r can be determined if the realized gain values of the transmitting horn antenna G_t and the receiving antenna G_r, the input power P_{in}, and the distance R between them are known.

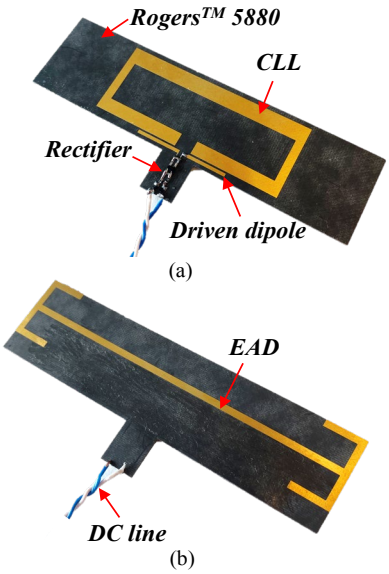

Fig. 7. Fabricated prototype of the electrically small single-substrate Huygens dipole rectenna. (a) Front view. (b) Back view.

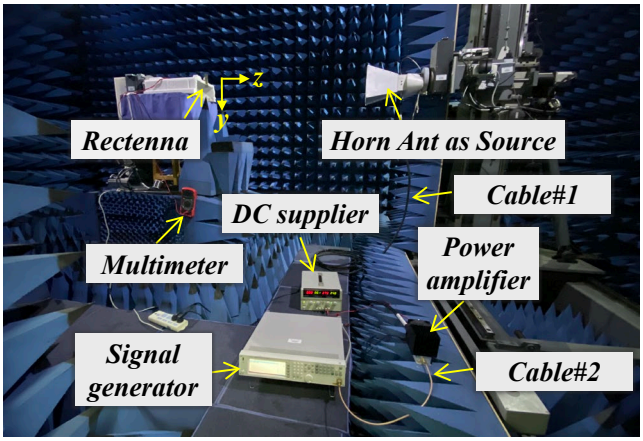

Fig. 8. Rectenna measurement setup in the anechoic chamber.

The distance R between the horn antenna and the rectenna in our customized measurement setup is 1.2 meters, which is in the far-field region of the horn antenna, i.e., greater than 0.55 meters at 915 MHz according to the $2D^2/\lambda_0$ value. The gain of the amplifier is 50.5 dB and the measured total loss from the two coaxial cables is 2.4 dB. Thus, the input power P_{in} is determined directly from the tunable output power strength of the signal generator. The realized gain values of the horn antenna G_t and the rectenna G_r are 7 dBi and 4.6 dBi, respectively. Consequently, the received power P_r is readily calculated from (1). The AC to DC conversion efficiency of the rectenna is determined by the ratio of the output DC power V_o^2/R_L and the received power P_r.

Fig. 9 gives the measured and simulated performance characteristics of the rectenna and the rectifier circuit. Fig. 9(a) shows the measured output DC voltage of the rectenna and the simulated realized gain values of the receiving HDA as functions of the source frequency. The measured peak output voltage value, 7.0 V, occurs at 909 MHz, indicating only a 6 MHz (0.7%) shift from simulated operating frequency, 915 MHz, as conveyed by the simulated realized gain values. Fig. 9(b) shows the measured and simulated output DC voltage values of the rectifier (circuit only) and the HLP rectenna as functions of the received power level. These values increase rapidly from a received power level of -10 dBm to become saturated above the 11 dBm level. The peak output voltage occurs when the received power P_r is 10.4 dBm (i.e., when the output power of the signal generator was set to -16 dBm).

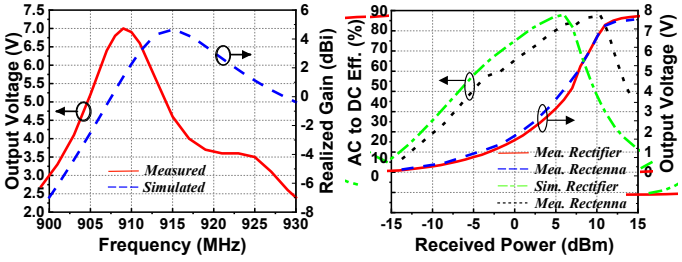

Fig. 9. Proof-of-concept results. (a) Measured output DC voltage as a function of the source frequency when the captured power is 10.4 dBm. (b) Measured and simulated output DC voltage values of the rectifier and the rectenna, and the AC to DC conversion efficiencies of the simulated rectifier and the measured rectenna as functions of the received power at 909 MHz.

Fig. 9(b) also presents the measured and simulated AC to DC conversion efficiencies at 909 MHz as functions of the received power. The measured peak value, 88%, also occurs when the received power is 10.4 dBm. Note that the AC to DC efficiency is above 50% in a wide range of received power, i.e., from -4 to 13 dBm. These results were obtained when the linear polarization of the rectenna was aligned with that of the horn field. The broadside direction of the rectenna, the z-axis in Fig. 1, pointed to the center of the horn. The HDA field is polarized along that y-axis, which is tangent to the rectenna surface. These axes are indicated again in Fig. 8.

To investigate the broad angle wireless power capture capability of the rectenna, its output was also measured for different angles of incidence. The output DC voltages at 909 MHz were 5.3, 6.6, 6.5, and 5.2 V, respectively, when the rectenna, i.e., its broadside direction, was rotated about the x-axis by -60˚, -30˚, +30˚, and +60˚ away from the line of sight to the horn. These results demonstrate the rectenna's broad angle wireless power capture capacity and high AC to DC conversion efficiency. Its ultra-compact size and excellent performance characteristics make the developed rectenna an ideal, attractive candidate for wirelessly powering IoT devices.

Note that all of the measured results are in good agreement with their simulated values. The circuit simulation results were obtained with the Advanced Design System (ADS) from Keysight Technologies™. The measured resonance frequency of the receiving HDA, 909 MHz, is a shift of only 6.0 MHz (0.7%) from the targeted and simulated operating frequency of 915 MHz. The slight shift in the received power that produces the highest conversion efficiency is due to the deviation of the actual component values of the Schottky diodes from their ADS models.

IV. Conclusion

The first realized electrically small single-substrate Huygens dipole rectenna was reported. The measured performance characteristics of their prototypes successfully demonstrated their quality and their agreement with their simulated values. They are ultra-compact, lightweight, and low cost. Table II summarizes a performance comparison of the developed rectenna with several previously reported examples including our own. It is clearly seen that the rectenna developed in this work is the only electrically small single-substrate design that simultaneously has a large realized gain, wide capture angle, and is easy to fabricate. Note that its peak realized gain is higher than our previously reported versions that were based on three PCB substrates. Its single-substrate design avoids the losses associated with the previous more complex layered structures. Given its exceptional performance characteristics, this innovative rectenna is a very attractive candidate for a variety of ultra-compact wireless power transfer (WPT) applications.

TABLE II:
Performance Comparison of Typical Examples of Previously Reported Rectennas

Ref.	Size (*ka*)	Realized gain of its antenna	Wireless power capture angle (HPBW)	Fabrication complexity
[7]	0.47*	1 dBi	N.A.	Easy (Single PCB)
[10]	1.2	3 dBi	90°	Moderate (Two PCBs)
[13]	3.07	8.6 dBi	60°	Moderate (Two PCBs)
[14]	1.46	2.3 dBi	81°	Easy (Single PCB)
[23]	0.73*	3.8 dBi	134˚ (± 67°)	Difficult (Three PCBs)
[24]	0.77*	3.3 dBic	134˚ (± 67°)	Difficult (Three PCBs)
This Work	**0.98***	**4.6 dBi**	**134˚ (± 67°)**	**Easy (Single PCB)**

* Electrically small when $ka < 1$, k being the wave number at resonance and a being the radius of the smallest sphere enclosing the entire structure.

V. Acknowledgements

The authors would like to thank Prof. Jianquan Huang, Xiangnan University, for his assistance in the measurement campaign; and Prof. Y. Jay Guo, University of Technology Sydney, for his support of these efforts.

References

[1] A. Costanzo and D. Masotti, "Energizing 5G: Near- and far-field wireless energy and data transfer as an enabling technology for the 5G IoT," *IEEE Microw. Mag.*, vol. 18, no. 3, pp. 125-136, May 2017.

[2] N. B. Carvalho, et al., "Wireless power transmission: R&D activities within Europe," *IEEE Trans. Microw. Theory Techn.*, vol. 62, no. 4, pp. 1031-1045, Apr. 2014.

[3] N. Shinohara, "Beam control technologies with a high-efficiency phased array for microwave power transmission in Japan," *Proc. IEEE*, vol. 101, no. 6, pp. 1448-1463, Jun. 2013.

[4] J. -H. Kim, Y. Lin, and S. Nam, "Efficiency bound of radiative wireless power transmission using practical antennas," *IEEE Trans. Antennas Propag.*, vol. 67, No. 8, pp. 5750-5755, Aug. 2019.

[5] A. Massa, G. Oliveri, F. Viani, and P. Rocca, "Array designs for long-distance wireless power transmission: State-of-the-art and innovative solutions," *Proc. IEEE*, vol. 101, no. 6, pp. 1464 - 1481, Jun. 2013.

[6] J. O. McSpadden, L. Fan, and K. Chang, "Design and experiments of a high conversion efficiency 5.8 GHz rectenna", *IEEE Trans. Microw. Theory Techn.,* vol.46, no.12, pp.2053- 2060, Dec. 1998.

[7] N. Zhu, R. W. Ziolkowski, and H. Xin, "A metamaterial-inspired, electrically small rectenna for high-efficiency low power harvesting and scavenging at the GPS L1 frequency," *Appl. Phys. Lett.*, vol. 99, 114101, Sep. 2011.

[8] A.Eid, J. Hester, J. Costantine, Y. Tawk, A. H. Ramadan, and M. M. Tentzeris, "A compact source-load agnostic flexible rectenna topology for IoT devices," *IEEE Trans. Antennas Propag.*, in early access, 2020.

[9] S. Shen, C.-Y. Chiu, and R. D. Murch, "Multiport pixel rectenna for ambient RF energy harvesting," *IEEE Trans. Antennas Propag.,* vol. 66, no. 2, pp. 644-656, Feb. 2018.

[10] M. Zeng, A. S. Andrenko, X. Liu, Z. Li, and H.-Z. Tan, "A compact fractal loop rectenna for RF energy harvesting," *IEEE Antennas Wirel. Propag. Lett.,* vol.16., pp. 2424 – 2427, 2017.

[11] Z. Gu, S. Hemour, L. Guo, and K. Wu, "Integrated cooperative ambient power harvester collecting ubiquitous radio frequency and kinetic energy," *IEEE Trans. Microw. Theory Techn.*, vol. 66, no. 9, pp. 4178-4190, Sep. 2018.

[12] C. Liu, Y. X. Guo, H. Sun, and S. Xiao, "Design and safety considerations of an implantable rectenna for far-field wireless power transfer," *IEEE Trans. Antennas Propag.*, vol. 62, no. 11, pp. 5798–5806, Nov. 2014.

[13] H. Sun, Y. X. Guo, M. He, and Z. Zhong, "Design of a high-efficiency 2.45-GHz rectenna for low-input-power energy harvesting," *IEEE Antennas Wireless Propag. Lett.*, vol. 11, pp. 929–932, 2012.

[14] V. Palazzi, et al., "A novel ultra-lightweight multiband rectenna on paper for RF energy harvesting in the next generation LTE bands," *IEEE Trans. Microw. Theory Techn.*, vol. 66, no. 1, pp. 366-379, Jan. 2018.

[15] C. Song, Y. Huang, P. Carter, J. Zhou, S. D. Joseph, and G. Li, "Novel compact and broadband frequency-selectable rectennas for a wide input-power and load impedance range," *IEEE Trans. Antennas Propag.*, vol. 66, no. 7, pp. 3306 – 3316, Jul. 2018.

[16] T. S. Almoneef, F. Erkmen, M. A. Alotaibi, and O. M. Ramahi, "A new approach to microwave rectennas using tightly coupled antennas," *IEEE Trans. Antennas Propag.*, vol. 66, no. 4, pp. 1714 – 1724, Apr. 2018.

[17] M. Mattsson, C. I. Kolitsidas, and B. L. G. Jonsson, "Dual-band dual-polarized full-wave rectenna based on differential field sampling," *IEEE Antennas Wirel. Propag. Lett.*, vol. 17, no. 6, pp. 956 – 959, Jun. 2018.

[18] Z. Popović, E. A. Falkenstein, D. Costinett, and R. Zane, "Low-power far-field wireless powering for wireless sensors," *Proc. IEEE*, vol. 101, no. 6, pp. 1397-1409, Jun. 2013.

[19] C. Song, et al., "A novel six-band dual CP rectenna using improved impedance matching technique for ambient RF energy harvesting," *IEEE Trans. Antennas Propag.,* vol. 64, no. 7, pp. 3160-3171, Jul. 2016.

[20] Z. Harouni, L. Cirio, L. Osman, A. Gharsallah, and O. Picon, "A dual circularly polarized 2.45-GHz rectenna for wireless power transmission," *IEEE Antennas Wirel. Propag. Lett.*, vol. 10, pp. 306 – 309, Apr. 2011.

[21] Y. Yang, et al., "A 5.8 GHz circularly polarized rectenna with harmonic suppression and rectenna array for wireless power transfer," *IEEE Antennas Wirel. Propag. Lett.,* vol. 17, no. 7, pp. 1276 – 1280, Jul. 2018.

[22] B. Strassner and K. Chang, "5.8-GHz circularly polarized rectifying antenna for wireless microwave power transmission," *IEEE Trans. Microw. Theory Techn.*, vol. 50, no. 8, pp. 1870-1876, Aug. 2002.

[23] W. Lin, R. W. Ziolkowski and J. Huang, "Electrically small, low profile, highly efficient, Huygens dipole rectennas for wirelessly powering Internet-of-Things (IoT) devices," *IEEE Trans. Antennas Propag.*, vol. 67, No. 6, pp. 3670-3679, June 2019.

[24] W. Lin, and R. W. Ziolkowski, "Electrically small Huygens circularly-polarized rectenna with delayed loop excitations," *IEEE Trans. Antennas Propag.*, vol. 68, No. 1, pp. 540-545, Jan. 2020.

[25] W. Lin, and R. W. Zolkowski, "Dual-functional electrically small Huygens antenna for wireless power transfer and communication applications," *IEEE Access*, vol. 7, pp. 39762-39769, Apr. 2019.

[26] R. W. Ziolkowski, "Low profile, broadside radiating, electrically small Huygens source antennas," *IEEE Access*, vol. 3, pp. 2644-2651, Dec. 2015.

[27] M. C. Tang, H. Wang and R. W. Ziolkowski, "Design and testing of simple, electrically small, low-profile, Huygens source antennas with broadside radiation performance," *IEEE Trans. Antennas Propag.*, vol. 64, no. 11, pp. 4607–4617, Nov. 2016.

[28] W. Lin and R. W. Ziolkowski, "Electrically-small, low-profile, Huygens circularly polarized antenna," *IEEE Trans. Antennas Propag*., vol. 66, no. 2, pp. 636-643, Feb. 2018.

[29] C. A. Balanis, 3rd Ed., *Antenna Theory*. New York: John Wiley & Sons, 2005.